Electronic Supplementary Information

Kinetics of Oxygen Surface Exchange on Epitaxial Ruddlesden-Popper Phases and Correlations to First-Principles Descriptors

Yueh-Lin Lee[1‡], Dongkyu Lee[1,2‡], Xiao Renshaw Wang[1], Ho Nyung Lee[2], Dane Morgan[3] and Yang Shao-Horn[1,*]*

[1]*Electrochemical Energy Laboratory, Massachusetts Institute of Technology, 77 Massachusetts Avenue, Cambridge, Massachusetts 02139, United States*

[2]*Materials Science and Technology Division, Oak Ridge National Laboratory, Oak Ridge, Tennessee 37831, United States*

[3]*Department of Materials Science and Engineering, University of Wisconsin–Madison, Madison, Wisconsin 53706, USA*

Index **Page**

Experimental - Normal X-ray diffraction (XRD) data of all films in Figure S1 clearly shows the presence of the $(00l)_{tetragonal}$ (l is integer) peaks of $La_{2-x}Sr_xMO_{4\pm\delta}$ and $(00l)_{cubic}$ (l is even) peaks of GDC and YSZ, indicating that all films are grown epitaxially with the *c*-axis perpendicular to the film surface. The in-plane crystallographic relationships between GDC and YSZ (a cube-on-cube alignment) and LSM_{214} and GDC (an in-plane 45° rotation) are revealed from off-normal phi scan in Figure S2. As shown in Table S1, the lattice mismatches between GDC and $La_{2-x}Sr_xMO_{4\pm\delta}$, do not change significantly with different cation substitutions ranging from -0.5 ~ -1.9%. The AFM images of the experimental *c*-axis oriented epitaxial RP_{214} thin film surfaces are provided in Figure S3.

The surface exchange coefficient (k_O^q) of all films are shown in Figure 1c of the main manuscript, where the anisotropic nature of oxygen surface exchange kinetics in RP_{214} oxides can be ruled out as a source of variation as all films were grown with the *c*-axis perpendicular to the film surface. The k_O^q values of epitaxial $LaSrCoO_{4\pm\delta}$ thin films were found to be ~2 orders of magnitude higher than those of $LaSrNiO_{4\pm\delta}$, which is in good agreement with that substituting Co for Ni can lead to enhance the oxygen surface exchange coefficient (k_O^*) in polycrystalline $La_2NiO_{4+\delta}$.[1]

It should be noted that the k_O^q values of $LaSrCoO_{4\pm\delta}$ thin films are found to be slightly lower than those of $La_2CuO_{4+\delta}$ thin films although $LaSrCoO_{4\pm\delta}$ contains a large amount of Sr (Sr=1.0) relative to $La_2CuO_{4+\delta}$. Furthermore, the k_O^q values of $La_{1.85}Sr_{0.15}CuO_{4\pm\delta}$ are found to not change significantly as Sr content increases to 0.4. Recently, we have shown that the k_O^q values of $La_{2-x}Sr_xNiO_{4\pm\delta}$ thin films can decrease with increasing Sr content due to the structure reorientation and the adsorption energy changes.[2] Boehm *et al.* have also reported that the Sr substitution (Sr = 0.1 and 0.2) can decrease the surface exchange kinetics of polycrystalline $La_2NiO_{4\pm\delta}$.[3] In contrast, the k_O^q values of the *c*-axis oriented $La_{2-x}Sr_xMO_{4\pm\delta}$ films were found to have no correlation with Sr content, as shown in Figure S5. Therefore, our observation suggests that the cation substitution on the M-site may play a more important role in the oxygen surface exchange kinetics of RP oxides compared to the Sr substitution on the A-site.

Computational approaches - Spin polarized Density Functional Theory (DFT) calculations are preformed with the Vienna *Ab-initio* Simulation Package[4] using the Projector-Augmented plane-Wave method.[5] Exchange-correlation is treated in the Perdew-Wang-91[6] Generalized Gradient Approximation (GGA). The GGA+*U* calculations are performed with the simplified spherically averaged approach, where the U_{eff} (U_{eff} = Coulomb *U* - exchange *J*) is applied to *d*-electrons. (U_{eff}(Co) = 3.3 eV, U_{eff}(Ni) = 6.4 eV, and U_{eff}(Cu) = 4.0 eV).[7] All calculations are performed in the ferromagnetic state in order to use a consistent and tractable set of magnetic structures and to provide a magnetic environment more similar to the application relevant high-temperature paramagnetic state than the (typically) antiferromagnetic ground state.[8]

Bulk calculations are performed using 56-atom tetragonal $2a \times 2a \times 1c$ supercells with lattice constants provided in Table S1. Coordinates of atoms are taken from those of the low temperature orthorhombic phases as initial atomic positions for relaxation,[9] in order to restore rotation and distortion of transition-metal-oxygen octahedra in the adopted tetragonal supercells. For the systems with Sr doping, Sr atoms are placed in the AO rocksalt layers with Sr^{2+}-Sr^{2+} distance as far as possible. An effective bulk O 2*p*-band center is determined using the mass centroid of the projected O *2p*-states (including both the occupied and unoccupied states) relative to the Fermi level of a relaxed stoichiometric RP_{214} supercell. The bulk oxygen defect formation energetics are calculated by referencing the total energy of the defect containing bulk supercells to that of the perfect bulk and the corrected O_2 gas phase energy (fitted with experimental formation enthalpies of a series of metal oxides), as described in Ref. [8]. The bulk oxygen defect configurations are provided in Figure S6.

RP_{214} (001) surfaces are simulated using the 9-layer 2×2 symmetric (001) AO terminated slabs (containing 84 atoms), as previously revealed to be the stable surface terminations from *ab initio* surface thermodynamic analysis for $LaSrCoO_4$[2] as well as from recent low-energy-ion-scattering (LEIS) measurements for (Pr, La)$_2NiO_{4+\delta}$ and $La_{2-x}Sr_xNiO_{4\pm\delta}$.[10] The surface models of the oxygen adsorption for O^{2-} and O^- as well as the surface oxygen vacancy formation are provided in Figure S7. The surface

adsorption and oxygen vacancy formation energies are also calculated using the corrected O_2 gas phase energy reference described above.

Correlation between the bulk O *2p-band* surface O defect energetics - To further demonstrate the capability of the bulk O *2p-band* center to correlate with the energetics of bulk and surface oxygen defect formation and surface oxygen adsorption, Figure S8(a) shows the bulk oxygen vacancy (blue empty circles), O^{2-} interstitial (brown filled circles) and O^{-} interstitial (red filled circles) formation energies vs. the computed bulk O *2p-band* center of a series of $La_{2-x}Sr_xMO_4$ (M=Co, Ni and Cu) phases. Oxygen vacancy formation energies and oxygen adsorption energies (the adsorbed O^{2-} and O^{-} species) of the ideal (001) AO surfaces vs. the computed bulk O *2p-band* center of $La_{2-x}Sr_xMO_4$ were plotted in Figure S8(b). Our results suggest that both the bulk and surface oxygen defect formation and surface oxygen adsorption energies correlate with the bulk O *2p-band* centers in a manner that suggests that the O *2p-band* centers is capturing with the essential physics governing the energy of the defect. For example, the opposite slope of the oxygen vacancy formation vs. the bulk O *2p-band* centers as compared to that of the O^{2-} interstitial formation in the bulk or O^{2-} adsorption on the surface is consistent with the opposite defect charge compensation of the two types of the oxygen defects: generation of electrons in oxygen vacancy formation while generation of holes in O^{2-} interstitials formation or surface O^{2-} adsorption). Furthermore, the almost flat slope of O^{-} interstitial formation in the bulk and O^{-} adsorption on the surface is also in a good agreement with no or very little charge exchange with the Fermi energy associated with formation of such peroxide oxygen species, *i.e.*, formation of O^{-} bound with a bulk or surface lattice oxygen causes no oxidation in the system: $\frac{1}{2}O_2(gas) + O^{2-}(lattice) \rightarrow O^{-}(interstitial) + O^{-}(lattice)$. While the existence of peroxide species in the RP_{214} phases has been reported in both experimental[11] and theoretical[12] studies, the role of O^{-} in surface exchange kinetics and bulk oxygen transport remains largely unclear. In this work, we mainly focus on the capability of the bulk O *2p-band* centers that consistently describe oxygen defect energetics both in the bulk and on the surface across various RP_{214} materials, and utilize its robustness to further capture trends associated with kinetics of oxygen surface exchange and bulk oxygen diffusion of the RP_{214} materials. .

Overall, the existence of the correlations between the bulk as well as the surface oxygen defect formation/oxygen adsorption and the computed bulk O *2p* band centers for a series of $La_{2-x}Sr_xMO_4$ phases suggests the averaged bulk O *2p-band* centers can effectively describe trends of both bulk and surface (for a specified surface orientation/facet) oxygen defect and adsorption energetics across various RP_{214} phases.

Surface exchange and oxygen diffusion along the (001) orientation - Although oxygen diffusion along the *a*-*b* plane (*i.e.*, the [100] or [010] directions) of the RP_{214} phases has been widely studied[13], mechanisms for oxygen transport (and surface exchange) along the *c*-axis direction (*i.e.,* the [001] direction) is less understood. Minervini *et al*.[13a] performed atomistic simulations with a Buckingham potential to investigate oxygen migration in $La_2NiO_{4+\delta}$, and reported a much greater activation barrier for oxygen transport *via* interstitialcy mechanism along the *c*-axis direction (~3 eV) vs. the *a*-*b* plane (0.3~0.9 eV) for O^{2-} and O^{-} interstitials. Such a significant difference in the calculated activation energies is in contrast to that of experimentally obtained activation barriers of oxygen diffusion in La_2NiO_4 single crystals[14] and epitaxial thin films[15], where the activation barriers of oxygen diffusion along the *c*-axis is comparable to or smaller than that along the *a*-*b* plane. Similar results were also reported for Pr_2NiO_4 and Nd_2NiO_4 single crystals[16] and crystallographically orientated La_2CuO_4 grains[17]. Bassat *et al.*[16] pointed out that, if the oxygen migration along the c-axis occurs through a direct vacancy mechanism, it would require significantly higher activation energy than that of the *a*-*b* planes. Therefore other transport mechanisms such as phonon assisted diffusion,[16] cooperative ionic transport across the perovskite layer[18], or participation of oxygen Frenkel defects and O^{-} species[14] (smaller ionic radii than O^{2-}) in the RP_{214} phases were proposed to be possible pathways for oxygen diffusion along the *c*-axis. Overall, these results indicate insufficient mechanistic understandings for oxygen transport along the *c*-axis direction in the RP_{214} phases, and also imply that presence of bulk oxygen understoichiometry such as $La_{1.5}Sr_{0.5}CuO_{4-\delta}$[19] and $LaSrNiO_{4-\delta}$[20] may not necessarily result in a direct oxygen vacancy mediated transport along the *c*-axis.

Material instability of the RP_{214} phases *vs.* the perovskite materials - We note that the experimental activation barriers of k_O* and D_O* for $La_2CoO_{4+\delta}$ are already close to 0 (see in Figure 4(a) of the main manuscript), and extrapolation of the O *2p-band* correlation to go beyond $La_2CoO_{4+\delta}$ for the RP_{214} materials will predict that these RP_{214} materials have negative activation barriers for their bulk oxygen transport and oxygen surface exchange, which indicates issues associated with material instability, since the energies of the transition states will become lower than those of the reactants. Indeed, it was reported by Munnings *et al.*[1] that no k_O* and D_O* data were obtained for temperatures above 684°C for the pure $La_2CoO_{4+\delta}$ sample due to the relative instability of this material at elevated temperatures in air, which leads to decomposition into $LaCoO_3$ and La_2O_3 at temperatures above ~700° C. Such a coupling between material catalytic activity and material instability is similar to the SOFC perovskite materials[21] (see discussions in Section 8 of the Supporting Information of Ref. [21]), where the more active SOFC perovskites are also less stable. However, the opposite trends (slopes) of oxygen surface exchange activity (as well as the activation barriers) vs. the bulk O *2p-band* centers (relative to the Fermi level) between the RP_{214} phase and the perovskites distinguish that both the material instability and the kinetics of oxygen surface exchange and bulk anionic transport are influenced by the intrinsic electronic structure properties, the bulk O *2p*-band centers, in the opposite manner.

Table S1. Lattice parameters of the experimental *c*-axis oriented epitaxial $La_{2-x}Sr_xMO_{4\pm\delta}$ (x = 0, 0.15, 0.4, 1 and M = Cu, Co, Ni) thin films on a $(001)_{cubic}$-YSZ substrate with a GDC (20 mol% Gd) as the buffer layer obtained from Normal X-ray diffraction (XRD).

Materials (bulk)	a_{bulk} /Å	c_{bulk} / Å	Substrate	Lattice mismatch (***a-b*** plane)
$La_{2-x}Sr_xCuO_{4\pm\delta}$, x=0[1)]	5.36	13.171	GDC (001), a_{GDC}= 5.418 Å[5)]	~ -1 %
			YSZ (001), a_{YSZ} = 5.147 Å[6)]	~ 3.9 %
$La_{2-x}Sr_xCuO_{4\pm\delta}$, x=0.15[2)]	3.78	13.238	GDC (001), a_{GDC}= 5.418 Å	~ -1.4 %
			YSZ (001), a_{YSZ} = 5.147 Å	~ 3.7 %
$La_{2-x}Sr_xCuO_{4\pm\delta}$, x=0.4[2)]	3.76	13.275	GDC (001), a_{GDC}= 5.418 Å	~ -1.9 %
			YSZ (001), a_{YSZ} = 5.147 Å	~ 3.2 %
$La_{2-x}Sr_xCoO_{4\pm\delta}$, x=1.0[3)]	3.807	12.507	GDC (001), a_{GDC}= 5.418 Å	~ -0.6 %
			YSZ (001), a_{YSZ} = 5.147 Å	~ 4.4 %
$La_{2-x}Sr_xNiO_{4\pm\delta}$, x=1.0[4)]	3.824	12.429	GDC (001), a_{GDC}= 5.418 Å	~ -0.2 %
			YSZ (001), a_{YSZ} = 5.147 Å	~ 4.8 %

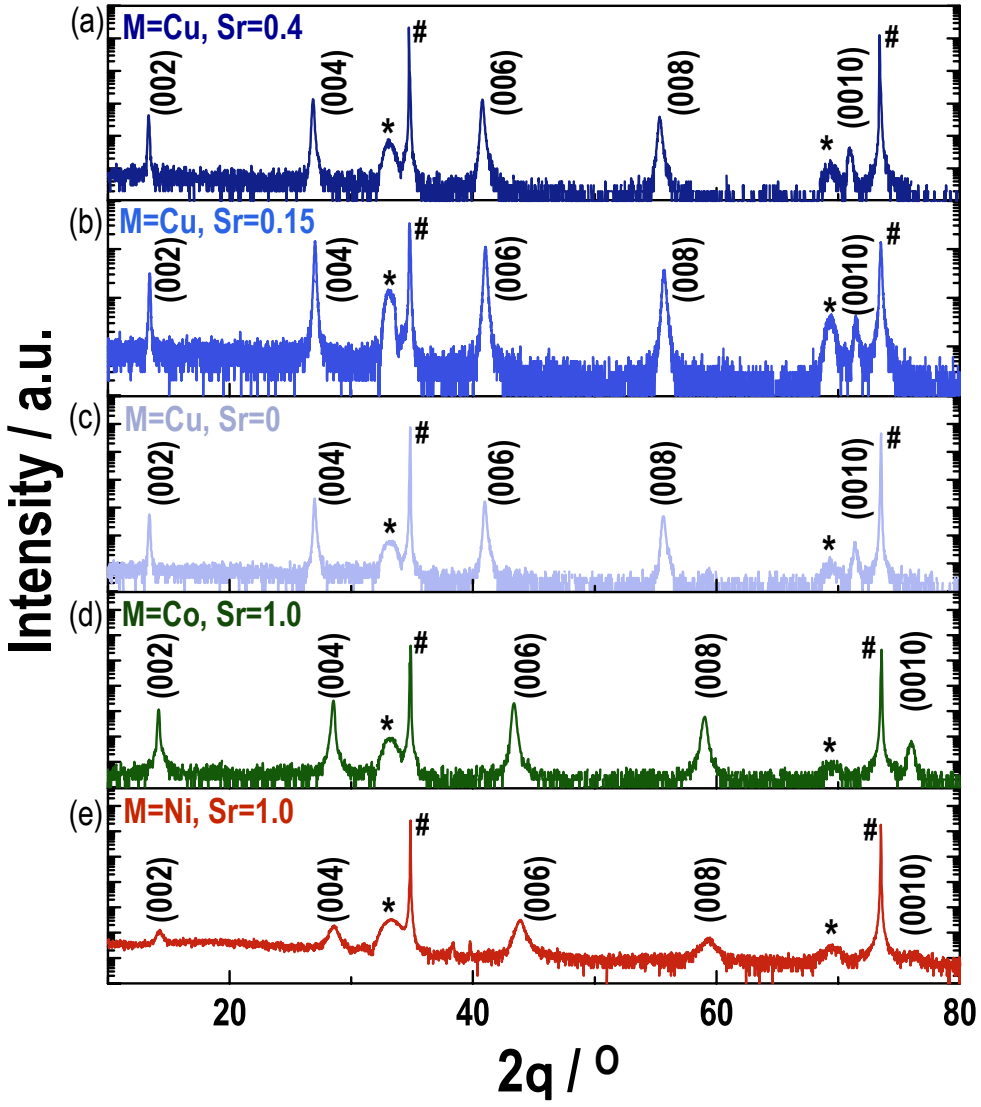

Figure S1. High-resolution X-ray diffraction analysis of (a) $La_{1.6}Sr_{0.4}CuO_{4\pm\delta}$, (b) $La_{1.85}Sr_{0.4}CuO_{4\pm\delta}$, (c) $La_2CuO_{4+\delta}$, (d) $LaSrCoO_{4\pm\delta}$, and (e) $LaSrNiO_{4\pm\delta}$ epitaxial thin films on (001) YSZ substrates with GDC buffer layer. YSZ substrate and GDC peaks are indicated with pounds (#) and asterisks (∗), respectively.

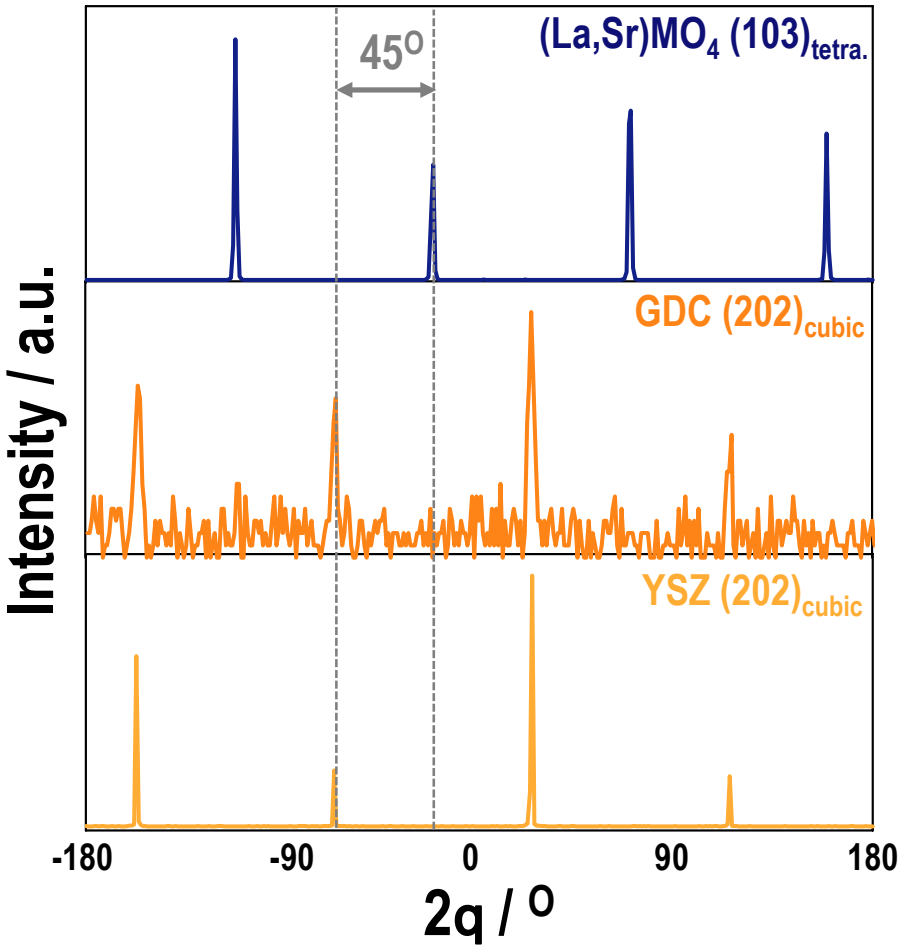

Figure S2. High-resolution X-ray diffraction analysis of (a) $La_{1.6}Sr_{0.4}CuO_{4\pm\delta}$, (b) $La_{1.85}Sr_{0.4}CuO_{4\pm\delta}$, (c) $La_2CuO_{4+\delta}$, (d) $LaSrCoO_{4\pm\delta}$, and (e) $LaSrNiO_{4\pm\delta}$ epitaxial thin films on (001) YSZ substrates with GDC buffer layer. YSZ substrate and GDC peaks are indicated with pounds (#) and asterisks (∗), respectively.

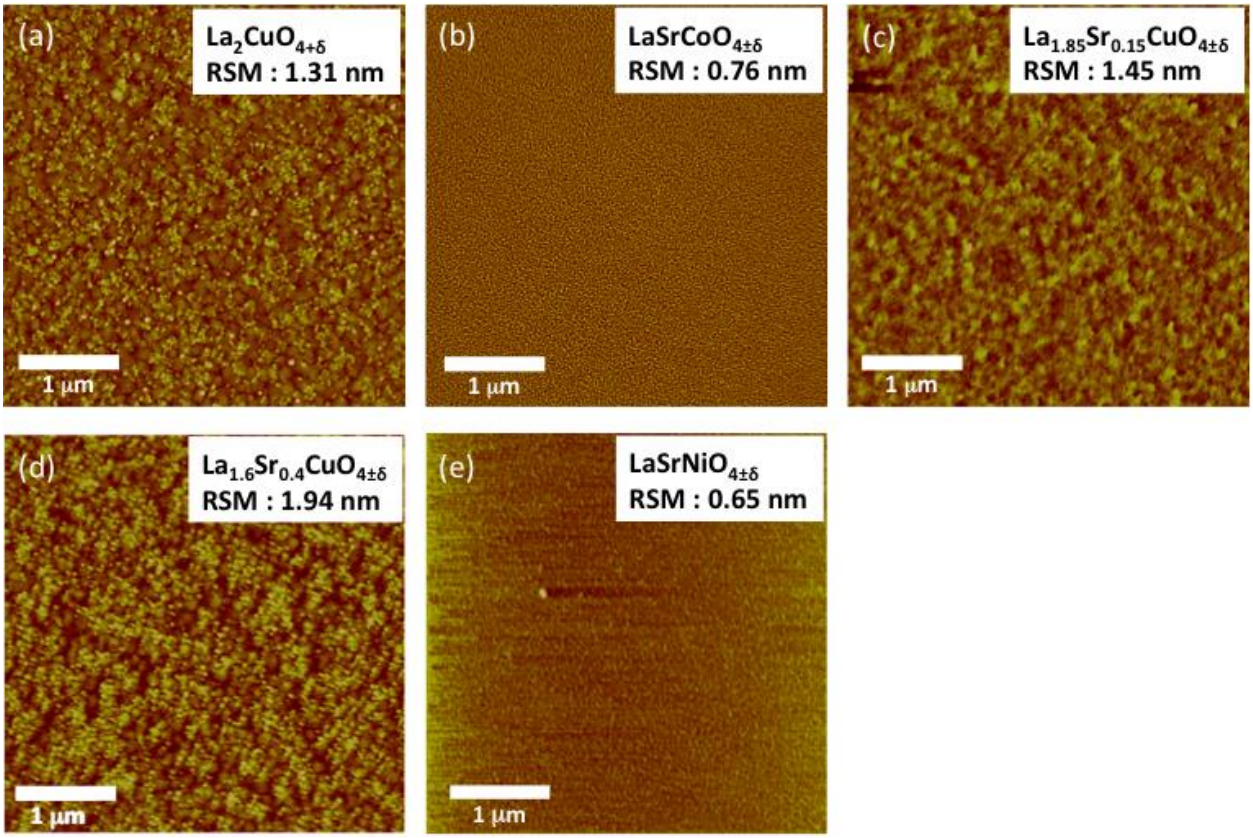

Figure S3. AFM images of the experimental *c*-axis oriented epitaxial RP_{214} thin film surfaces of (a) $La_2CuO_{4+\delta}$ (b) $LaSrCoO_{4\pm\delta}$ (c) $La_{1.85}Sr_{0.15}CuO_{4\pm\delta}$ (d) $La_{1.6}Sr_{0.4}CuO_{4\pm\delta}$ and (e) $LaSrNiO_{4\pm\delta}$.

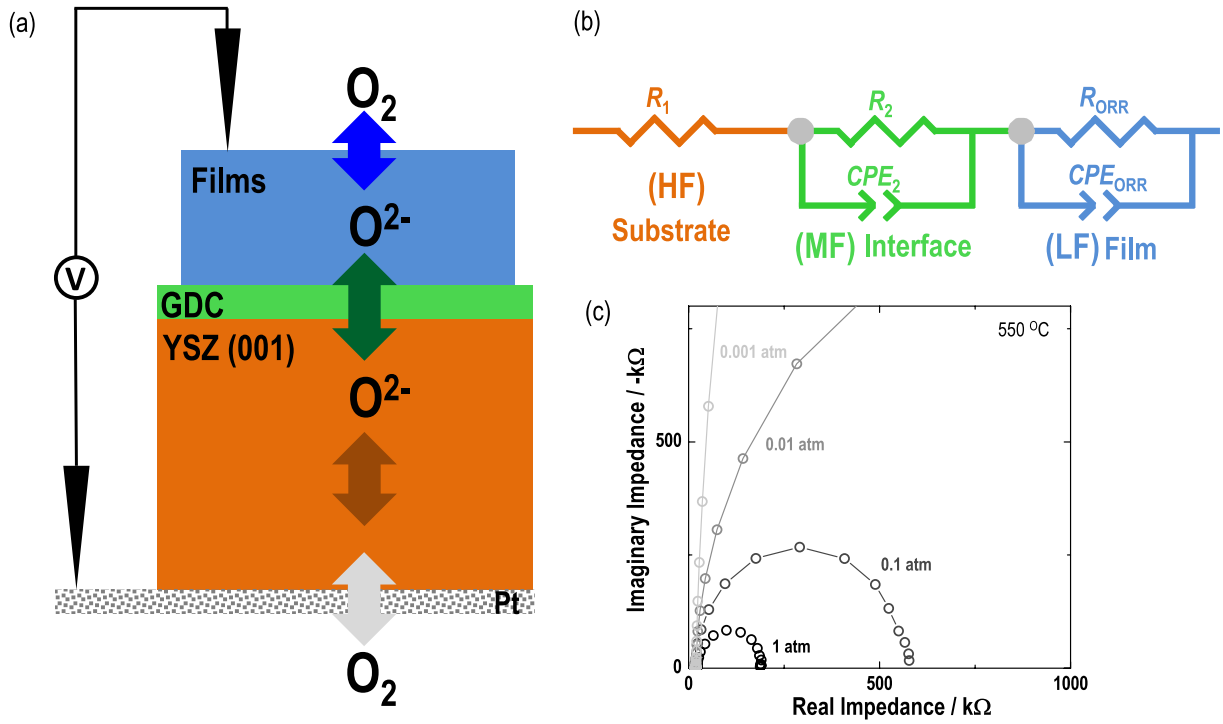

Figure S4. (a) Schematic of a LNO/GDC/YSZ(001)/porous Pt samples and electrochemical testing configuration (not drawn to scale), and (b) equivalent circuit (R1 = YSZ electrolyte resistance, R2 = electrode/electrolyte interface resistance4, RORR = ORR resistance, CPE = constant phase element) used to extract ORR kinetics, and (c) Nyquist plot of the $La_2CuO_{4\pm\delta}$ thin films at 550 ºC;

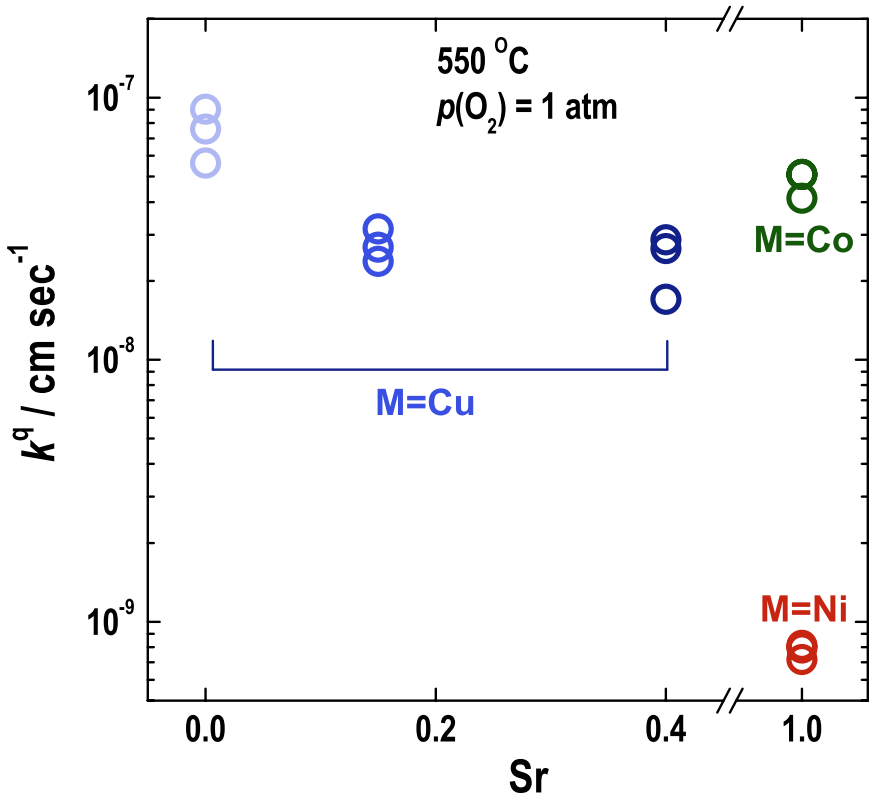

Figure S5. Sr content dependency of the surface exchange coefficients of $La_2CuO_{4+\delta}$ (light blue), $LaSrCoO_{4\pm\delta}$, (green), $La_{1.85}Sr_{0.4}CuO_{4\pm\delta}$ (blue) ,$La_{1.6}Sr_{0.4}CuO_{4\pm\delta}$ (deep blue) and $LaSrNiO_{4\pm\delta}$ (red) thin films calculated from electrochemical impedance spectroscopy (EIS) spectra collected at 550 ^{O}C. Three microelectrodes from each sample were measured at the same oxygen partial pressure.

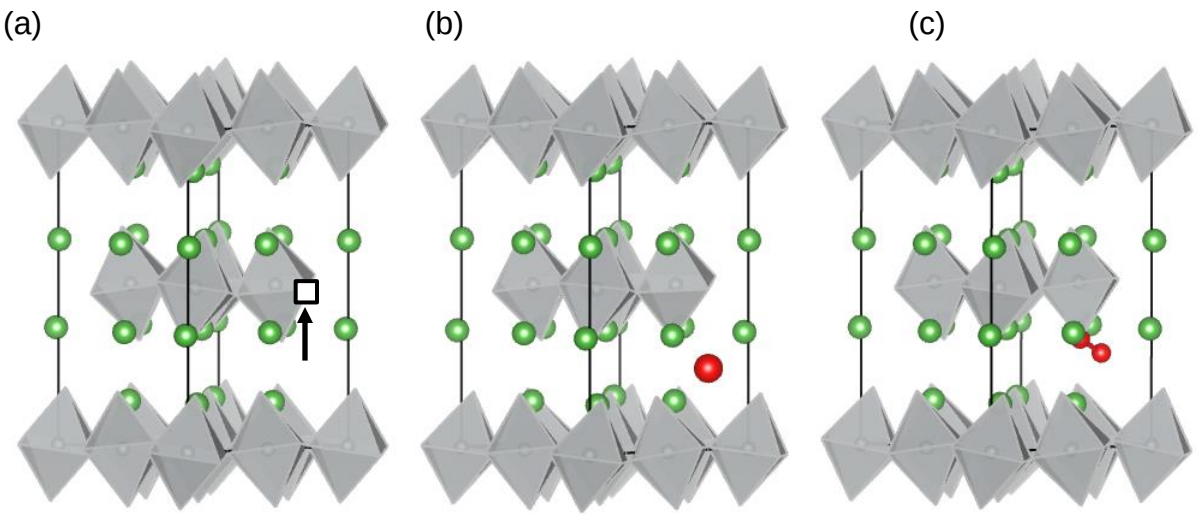

Figure S6. The simulated RP_{214} configurations of bulk (a) oxygen vacancy formation (b) O^{2-} interstitial formation (c) O^{-} interstitial formation. The green circles represent A site (for La or Sr) and the grey octahedra represent the M-O local environment (M=Co, Ni, and Cu). The empty square in Figure S6(a), the large red circles in Figure S6(b), and the small red circles in Figure S6(c) are the oxygen vacancy, O^{2-} interstitial, and O^{-} interstitial bound with an apical lattice oxygen, respectively. The O-O bond distance between the O^{-} interstitial and the nearest neighbor oxygen is 1.5~1.6 Å.

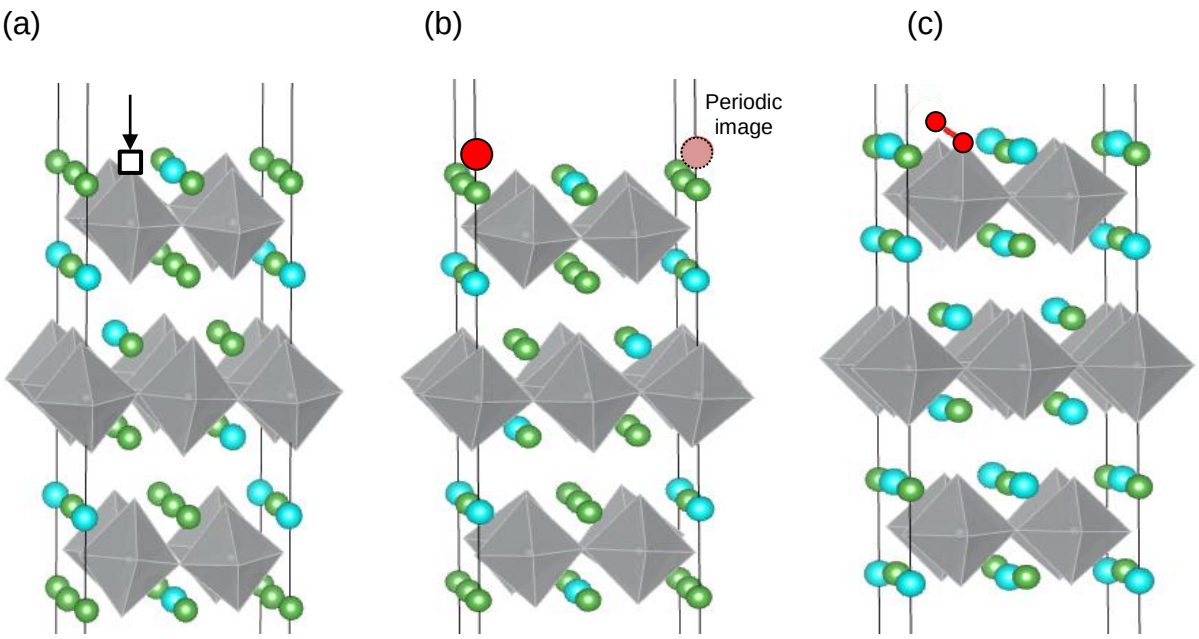

Figure S7. Simulated configurations of (a) surface oxygen vacancy (b) surface adsorbed O^{2-} (c) surface adsorbed O^{-} on the (001) AO terminated surfaces of the RP_{214} 9-layer 2×2 symmetric slabs. The green circles represent La^{3+} and blue circles represent Sr^{2+} and the grey octahedra represent the M-O local environment (M=Co, Ni, and Cu). The empty square in Figure S7(a), the large red circles in Figure S7(b), and the small red circles in Figure S7(c) are the oxygen vacancy, O^{2-} interstitial, and O^{-} interstitial bound with a surface apical oxygen, respectively. Again, the O-O bond distance between the surface adsorbed O^{-} and the nearest neighbor oxygen is 1.5~1.6 Å.

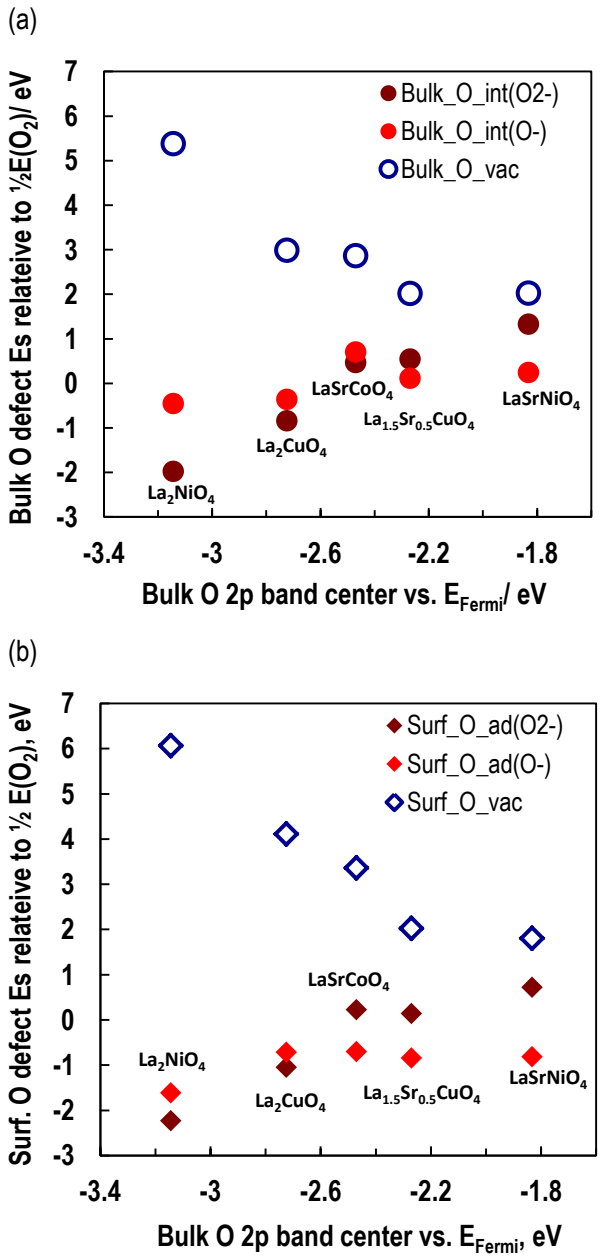

Figure S8. (a) The computed DFT bulk oxygen defect energetics for formation of an oxygen vacancy in the MO_2 layer (blue empty circles), an O^{2-} interstitial in the A_2O_2 layer (filled brown circles), and an O^- interstitial bound with an apical oxygen in the A_2O_2 layer (filled red circels) vs. the bulk O *2p-band* centers (relative to the Fermi level, E_{Fermi}) for La_2NiO_4, La_2CuO_4, $LaSrCoO_4$, $La_{1.5}Sr_{0.5}CuO_4$ and $LaSrNiO_4$. The simulated configurations are provided in Figure S7(a). (b) The computed DFT surface oxygen defect and oxygen adsorption energetics for formation of an oxygen vacancy at the top AO surface layer (blue empty diamonds), and surface adsorbed O^{2-} (filled brown diamond), and adsorbed O^- (filled red diamond)vs. the bulk O *2p-band* centers (relative to the Fermi level, E_{Fermi}) for La_2NiO_4, La_2CuO_4, $LaSrCoO_4$, $La_{1.5}Sr_{0.5}CuO_4$ and $LaSrNiO_4$.

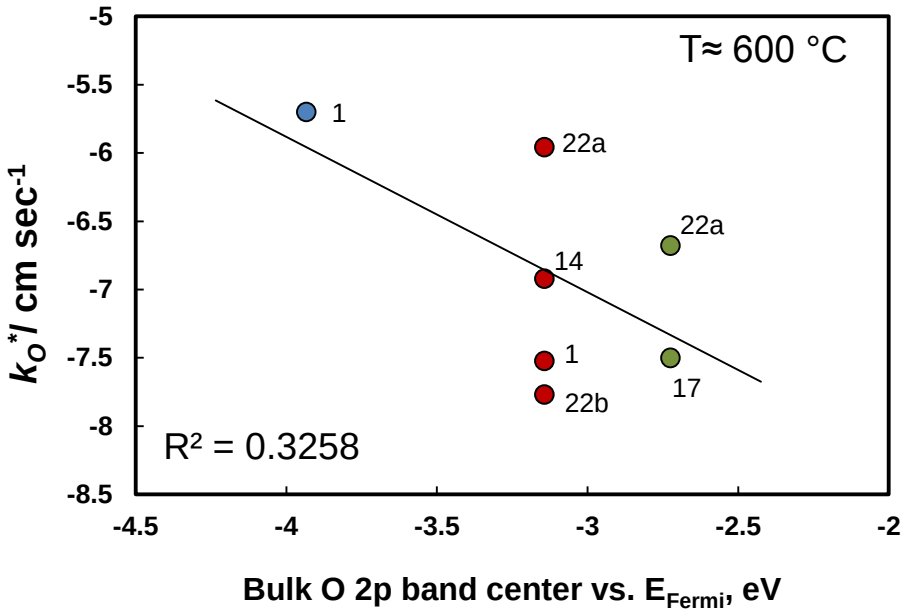

Figure S9. Experimental oxygen surface exchange coefficients (k_O^*) at T≈ 600 °C from the literature vs. the computed bulk O *2p*-band center for $La_2CoO_{4+\delta}$ (blue),[1] $La_2NiO_{4+\delta}$ (red),[1, 14, 22] and $La_2CuO_{4+\delta}$ (green).[17, 22a]. Labels near the data points indicate the corresponding references where the experimental k_O^*s are taken.

References:

1. Munnings, C. N.; Skinner, S. J.; Amow, G.; Whitfield, P. S.; Davidson, I. J., Oxygen transport in the La2Ni1-xCoxO4+d system. *Solid State Ionics* **2005,** *176* (23¸Äì24), 1895-1901.

2. Lee, D.; Lee, Y.-L.; Hong, W. T.; Biegalski, M. D.; Morgan, D.; Shao-Horn, Y., Oxygen surface exchange kinetics and stability of (La,Sr)2CoO4+/-[small delta]/La1-xSrxMO3-[small delta] (M = Co and Fe) hetero-interfaces at intermediate temperatures. *Journal of Materials Chemistry A* **2015,** *3* (5), 2144-2157.

3. Boehm, E.; Bassat, J. M.; Dordor, P.; Mauvy, F.; Grenier, J. C.; Stevens, P., Oxygen diffusion and transport properties in non-stoichiometric Ln2 − xNiO4 + δ oxides. *Solid State Ionics* **2005,** *176* (37–38), 2717-2725.

4. (a) Kresse, G.; Hafner, J., Ab initio molecular dynamics for liquid metals. *Physical Review B* **1993,** *47*, 558; (b) Kresse, G.; Furthmuller, J., Efficient iterative schemes for ab initio total-energy calculations using a plane-wave basis set. *Physical Review B* **1996,** *54* (16), 11169-11186.

5. Blochl, P. E., PROJECTOR AUGMENTED-WAVE METHOD. *Physical Review B* **1994,** *50* (24), 17953-17979.

6. Perdew, J. P.; Wang, Y., Accurate and simple analytic representation of the electron-gas correlation energy. *Physical Review B* **1992,** *45* (Copyright (C) 2010 The American Physical Society), 13244.

7. Wang, L.; Maxisch, T.; Ceder, G., Oxidation energies of transition metal oxides within the GGA+U framework. *Physical Review B* **2006,** *73* (19), 195107.

8. Lee, Y.-L.; Kleis, J.; Rossmeisl, J.; Morgan, D., Ab initio energetics of LaBO[sub 3](001) (B = Mn, Fe, Co, and Ni) for solid oxide fuel cell cathodes. *Physical Review B (Condensed Matter and Materials Physics)* **2009,** *80* (22), 224101.

9. Jorgensen, J. D.; Dabrowski, B.; Pei, S.; Richards, D. R.; Hinks, D. G., Structure of the interstitial oxygen defect in La2NiO4+delta. *Physical Review B* **1989,** *40* (4), 2187-2199.

10. (a) Druce, J.; Ishihara, T.; Kilner, J., Surface composition of perovskite-type materials studied by Low Energy Ion Scattering (LEIS). *Solid State Ionics* (in press, 2013); (b) Burriel, M.; Wilkins, S.; Hill, J. P.; Munoz-Marquez, M. A.; Brongersma, H. H.; Kilner, J. A.; Ryan, M.

P.; Skinner, S. J., Absence of Ni on the outer surface of Sr doped La2NiO4 single crystals. *Energy & Environmental Science* **2014,** *7* (1), 311-316.

11. (a) Buttrey, D. J.; Ganguly, P.; Honig, J. M.; Rao, C. N. R.; Schartman, R. R.; Subbanna, G. N., Oxygen excess in layered lanthanide nickelates. *Journal of Solid State Chemistry* **1988,** *74* (2), 233-238; (b) Li, Z. G.; Feng, H. H.; Yang, Z. Y.; Hamed, A.; Ting, S. T.; Hor, P. H.; Bhavaraju, S.; DiCarlo, J. F.; Jacobson, A. J., Carrier-Controlled Doping Efficiency in La2CuO4+delta. *Phys. Rev. Lett.* **1996,** *77* (27), 5413-5416.

12. Lee, K. H.; Hoffmann, R., Oxygen Interstitials in Superconducting La2CuO4: Their Valence State and Role†. *The Journal of Physical Chemistry A* **2006,** *110* (2), 609-617.

13. (a) Minervini, L.; Grimes, R. W.; Kilner, J. A.; Sickafus, K. E., Oxygen migration in La2NiO4+δ. *J. Mater. Chem.* **2000,** *10* (10), 2349-2354; (b) Chroneos, A.; Parfitt, D.; Kilner, J. A.; Grimes, R. W., Anisotropic oxygen diffusion in tetragonal La2NiO4+[small delta]: molecular dynamics calculations. *J. Mater. Chem.* **2010,** *20* (2), 266-270; (c) Parfitt, D.; Chroneos, A.; Kilner, J. A.; Grimes, R. W., Molecular dynamics study of oxygen diffusion in Pr2NiO4+[small delta]. *Physical Chemistry Chemical Physics* **2010,** *12* (25), 6834-6836; (d) Kushima, A.; Parfitt, D.; Chroneos, A.; Yildiz, B.; Kilner, J. A.; Grimes, R. W., Interstitialcy diffusion of oxygen in tetragonal La2CoO4+[small delta]. *Physical Chemistry Chemical Physics* **2011,** *13* (6), 2242-2249.

14. Bassat, J. M.; Odier, P.; Villesuzanne, A.; Marin, C.; Pouchard, M., Anisotropic ionic transport properties in La2NiO4+delta single crystals. *Solid State Ionics* **2004,** *167* (3-4), 341-347.

15. Burriel, M.; Garcia, G.; Santiso, J.; Kilner, J. A.; Richard, J. C. C.; Skinner, S. J., Anisotropic oxygen diffusion properties in epitaxial thin films of La2NiO4+delta. *J. Mater. Chem.* **2008,** *18* (4), 416-422.

16. Bassat, J.-M.; Burriel, M.; Wahyudi, O.; Castaing, R.; Ceretti, M.; Veber, P.; Weill, I.; Villesuzanne, A.; Grenier, J.-C.; Paulus, W.; Kilner, J. A., Anisotropic Oxygen Diffusion Properties in Pr2NiO4+δ and Nd2NiO4+δ Single Crystals. *The Journal of Physical Chemistry C* **2013,** *117* (50), 26466-26472.

17. Claus, J.; Borchardt, G.; Weber, S.; Hiver, J.-M.; Scherrer, S., Combination of EBSP measurements and SIMS to study crystallographic orientation dependence of diffusivities in a

polycrystalline material: oxygen tracer diffusion in La2 − xSrxCuO4 ± δ. *Materials Science and Engineering: B* **1996,** *38* (3), 251-257.

18. Naumovich, E. N.; Kharton, V. V., Atomic-scale insight into the oxygen ionic transport mechanisms in La2NiO4-based materials. *Journal of Molecular Structure: THEOCHEM* **2010,** *946* (1–3), 57-64.

19. Kanai, H.; Mizusaki, J.; Tagawa, H.; Hoshiyama, S.; Hirano, K.; Fujita, K.; Tezuka, M.; Hashimoto, T., Defect Chemistry of La2−xSrxCuO4−δ: Oxygen Nonstoichiometry and Thermodynamic Stability. *Journal of Solid State Chemistry* **1997,** *131* (1), 150-159.

20. Vashook, V. V.; Trofimenko, N. E.; Ullmann, H.; Makhnach, L. V., Oxygen nonstoichiometry and some transport properties of LaSrNiO4−δ nickelate. *Solid State Ionics* **2000,** *131* (3–4), 329-336.

21. Lee, Y.-L.; Kleis, J.; Rossmeisl, J.; Shao-Horn, Y.; Morgan, D., Prediction of solid oxide fuel cell cathode activity with first-principles descriptors. *Energy & Environmental Science* **2011,** *4* (10), 3966-3970.

22. (a) Boehm, E.; Bassat, J. M.; Steil, M. C.; Dordor, P.; Mauvy, F.; Grenier, J. C., Oxygen transport properties of La2Ni1−xCuxO4+δ mixed conducting oxides. *Solid State Sci.* **2003,** *5* (7), 973-981; (b) Sayers, R.; De Souza, R. A.; Kilner, J. A.; Skinner, S. J., Low temperature diffusion and oxygen stoichiometry in lanthanum nickelate. *Solid State Ionics* **2010,** *181* (8–10), 386-391.